https://doi.org/10.1007/s11467-022-1179-9

RESEARCH ARTICLE

Digital coding transmissive metasurface for multi-OAM-beam

Si Jia Li[1,2,3,†], Zhuo Yue Li[1], Guo Shai Huang[1], Xiao Bin Liu[1], Rui Qi Li[2], Xiang Yu Cao[1,3]

[1]*Information and Navigation College, Air Force Engineering University, Xi'an 710077, China*
[2]*State Key Laboratory of Millimeter Waves, School of Information Science and Engineering, Southeast University, Nanjing 210096, China*
[3]*Shaanxi Key Laboratory of Artificially-Structured Functional Materials and Devices, Air Force Engineering University, Xi'an 710051, China*
Corresponding author. E-mail: †lsj051@126.com
Received March 9, 2022; accepted May 16, 2022

Supporting Information

Digital coding transmissive metasurface for multi-OAM-beam

Design principles and spectrum of DCTMS element

The DCTMS can realize the multi-OAM-beam in free-space which reveals the strong power of controlling EM wave. To realize the function, the DCTMS is designed and simulated to satisfy the continuous phase variation. Figure S1 demonstrates the surface current distribution and spectrum of incident characteristics of proposed element. Figs. S1(a-d) show the surface current distribution on top and bottom layers at 9.3 GHz respectively. The surface current distributions with *x*-polarization incidences are displayed in Figs. S1(a, b). It can be seen that the surface current mainly flows along the titled arms at top layer. The surface current on bottom layer is induced with same direction when it is excited on the top layer. Furthermore, the opposite results can be found with *y*-polarized incident waves due to the symmetrical micro-structure of unit cell. Figures S1(c, d) reveal the surface current distribution with *y*-polarized incidence. The surface current is mainly excited on the incline arms at top layer while it is induced with adverse direction on bottom layer, which tend to generate 180deg phase difference.

The spectrum in Figs. S1(e-i) investigates the incident characteristics of proposed element, the transmissive coefficients and phase difference are calculated with different incident angle theta correspond to spherical coordinate. From Figs. S1(e, f), it is noted that the transmissive coefficient of $|t_{xx}|$ and $|t_{yy}|$ is near to 0.8 in 9.2-9.4 GHz when incident angle theta alters from -75° to 75°. Figures S1(g-i) show the co-polarized transmissive phase Φ_{xx}, Φ_{yy} and phase difference $\Delta\Phi=\Phi_{xx}-\Phi_{yy}$. Analogously, it is obvious that the phase difference is close to 180° with different incident angles, which demonstrated the insensible transmission. Spectrums of element are displayed the characteristics of wide incident transmission. Based on all mentioned above, the element can realize wide incident transmission in 9.2-9.4 GHz as incident angle shifts from -75° to 75°.

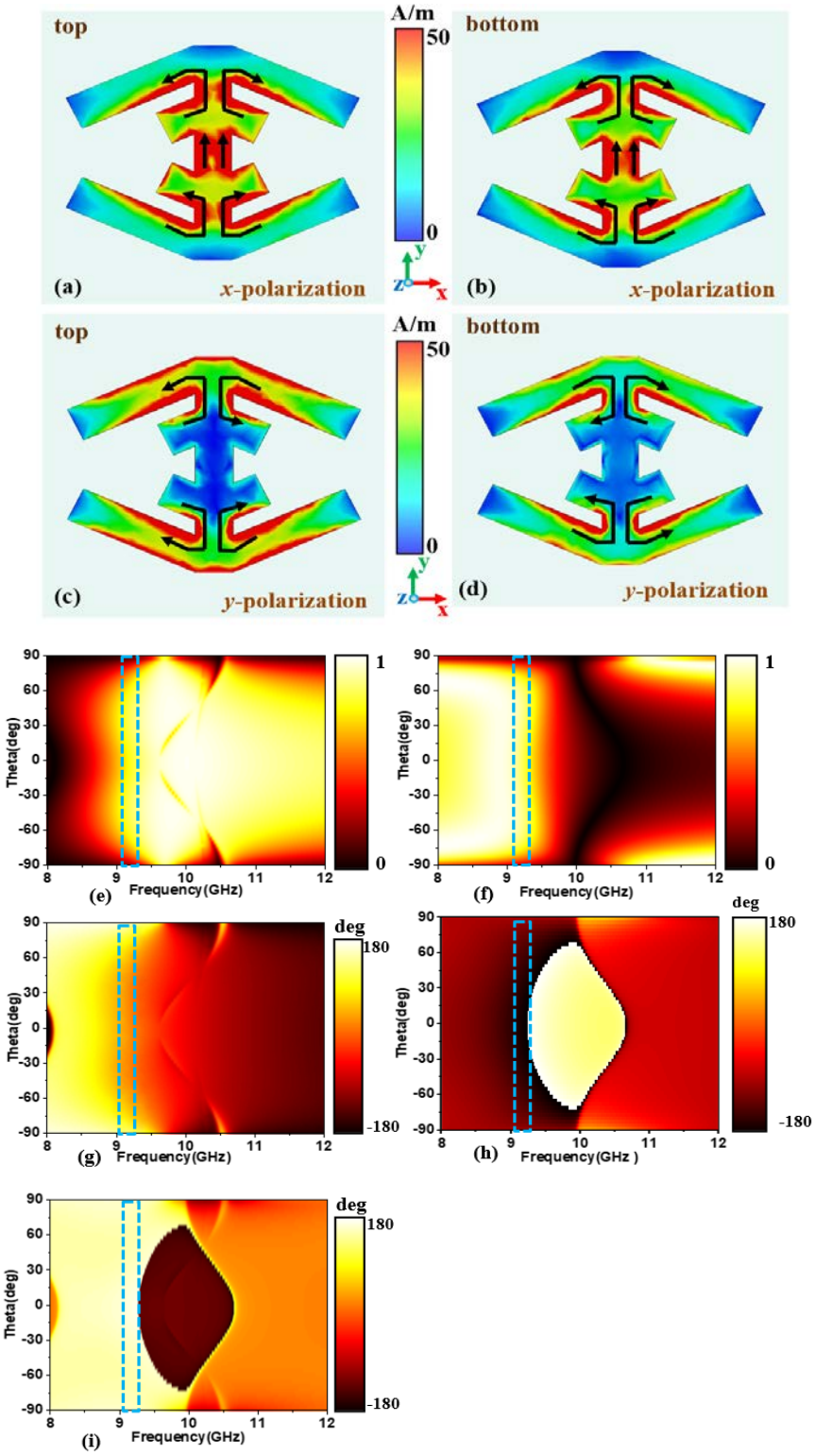

Fig. S1 The surface current distribution and spectrum of incident characteristics of proposed element. **(a, b)** The surface current distributions on top and bottom views with *x*-polarized incidence at 9.3 GHz. **(c, d)** The surface current distributions on top and bottom views with *y*-polarized incidence at 9.3 GHz. **(e, f)** The co-polarized transmission of t_{xx} with *x*-polarized incidence and t_{yy} with *y*-polarized incidence when incident angle theta alters from -90° to 90°. **(g)** The co-polarized transmissive phase Φ_{yy} with *y*-polarized incidence when incident angle theta alters from -90°to 90°. (h) The co-polarized transmissive phase Φ_{xx} with *x*-polarized incidence when incident angle theta alters from -90° to 90°. (i) The phase difference $\Delta\Phi$ of

Φ_{xx} and Φ_{yy} when incident angle theta alters from -90° to 90°.

Schematic of coding sequence for multi-OAM-beam

The coding sequence of multi-OAM-beam are achieved by convolution theorem. For realizing multi-function of results, the coding sequence is operated by adding results of coding sequence and modulus with 2^N, where N is bit number of coding sequence. As shown in Fig. S2(a), the coding sequence of single-OAM-beam are achieved by coding sequence of -2 mode OAM and phase compensation. To generate dual-OAM-beam, the coding sequence of "44440000" is introduced in the manuscript for beam split. The coding sequence of dual-OAM-beam are consisted of -2 mode OAM coding sequence, phase compensation coding sequence and "44440000" beam split coding sequence in Fig. S2(b). Similarly, the coding sequence of quad-OAM-beam is operated by the sequence of -2 mode OAM coding sequence, phase compensation coding sequence and "44440000" beam split coding sequence along x-axis direction and y-axis direction which is revealed in Fig. S2(c).

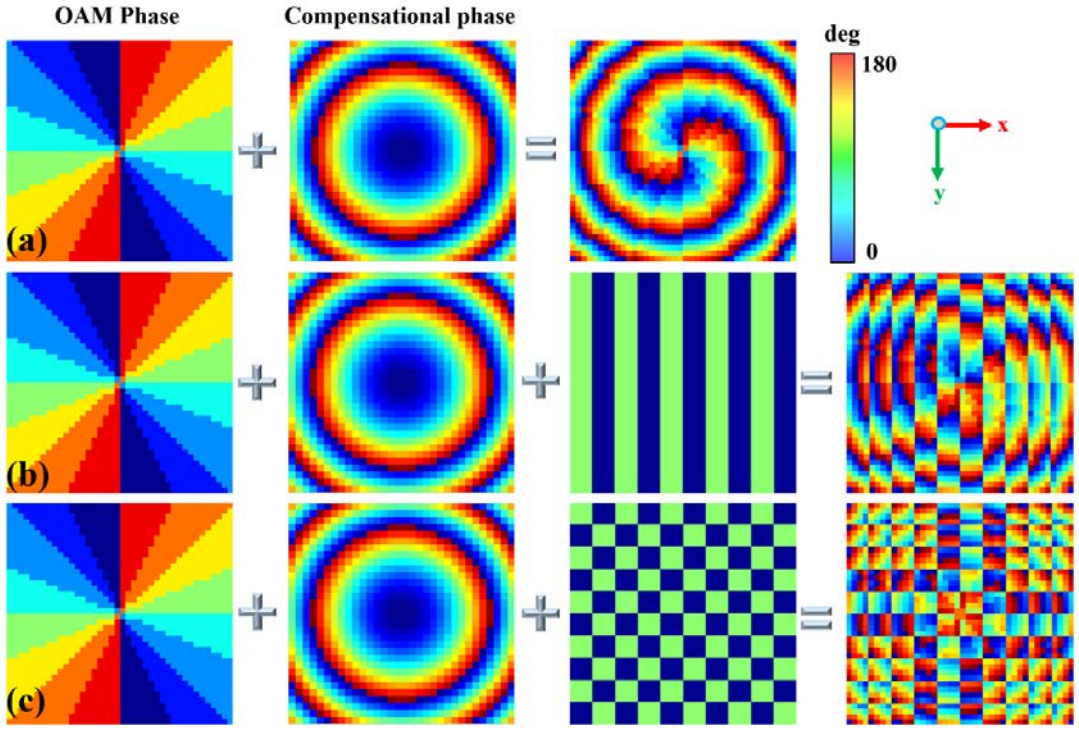

Fig. S2 The schematic of multi-OAM-beam with -2 mode for DCTMS. **(a)** Coding patterns of single-OAM-beam. **(b)** Coding patterns of dual-OAM-beam. **(c)** Coding patterns of quad-OAM-beam.

Results of quad-OAM-beam at 9.2 GHz and 9.4 GHz

To explore the performance of designed metasurface for quad-OAM-beam in 9.2-9.4 GHz, the results of quad-beam for OAM in spherical coordinate system. The quad-OAM-beam with doughnut shape magnitude distribution are revealed in Fig. S3. The phase distribution verifies the -2mode OAM which is corresponding to the magnitude distribution. Moreover, the magnitude at 9.2 GHz and 9.4GHz is lower than that of 9.3 GHz, this is because the results at 9.3 GHz has highest transmission coefficiency which lead to perfect performance. The results of quad-OAM-beam have been proved in 9.2-9.4 GHz.

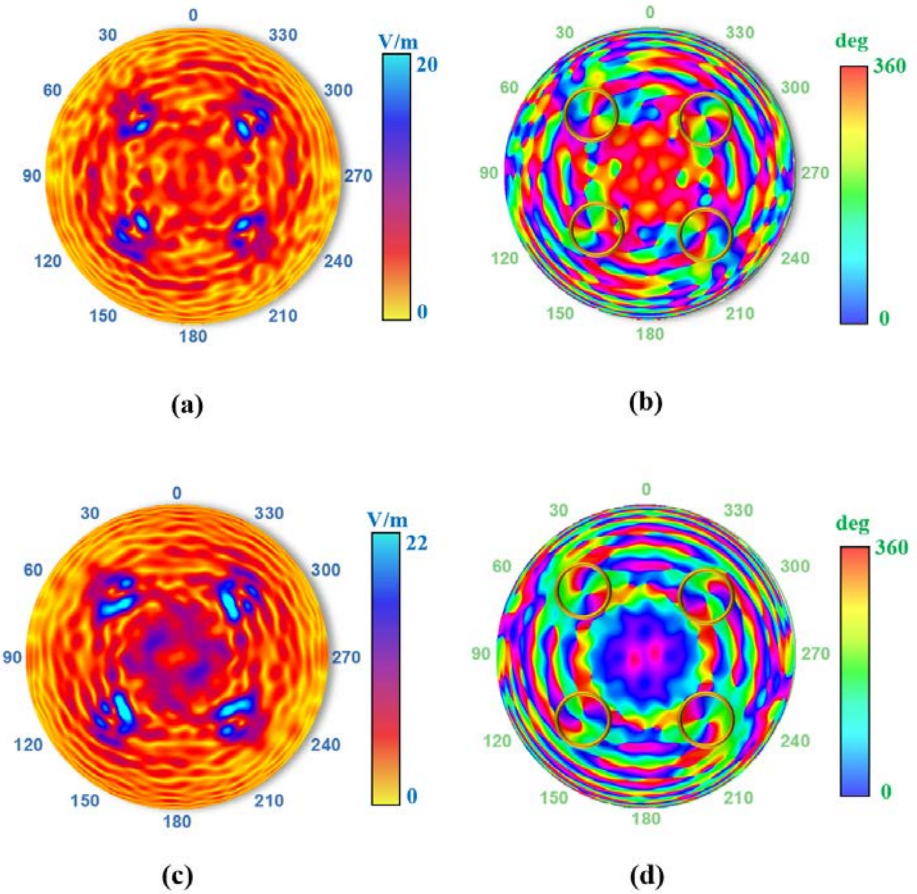

Fig. S3 The results of quad-beam for OAM in spherical coordinate system at 9.2 GHz and 9.4 GHz. **(a, b)** The simulated magnitude and phase distributions at 9.2 GHz. **(c, d)** The Simulated magnitude and phase distributions at 9.4 GHz.

Three prototypes of DCTMS

To demonstrate the transmissive metasurface, three prototypes of DCTMS with different characteristics are composed of 1600 unit cells as shown in Fig. S4. The substrates of F4B with permittivity of 3.7 and loss tangent of 0.004 were fabricated by printed circuit board technology. The experimental far-field and near-field results for these prototypes are all measured in a microwave anechoic chamber. A linearly polarized standard-gain horn antenna for emission, which covers 8-12 GHz, was connected to one port of a vector network analyzer (Agilent N5230C) for radiating the EM waves. The right-hand circularly polarized horn antenna for receiver was successively connected to the other port of the vector network analyzer. These prototypes are all placed z_f=300 mm away from the emissive antenna. The prototypes and emissive antenna were placed vertically in the center of a turntable to ensure that the EM wave could be similar to a plane wave on the front of prototype. Furthermore, the circularly polarized horn antenna was putted 10 m away from the prototypes. The distance between CP horn antenna and prototypes under test satisfied the far-field condition.

To measure the near electric fields, an appropriate waveguide port serving as the probe was motivated by the automatic test system. The distance of 20 mm between the probe and the DCTMS prototype has been chosen in the microwave anechoic chamber. However, due to the beam of dual-OAM and quad-OAM have certain deflection angle, the prototypes have been

rotated to ensure the OAM beam perpendicular to the test probe. Moreover, the distance of 200 mm has been adopted for the DCTMS prototypes with dual-OAM-beam and quad-OAM-beam. The measured results are the same as simulated results which verify the method for multi-OAM-beam generation. The sampling interval of 10 mm has been chosen to satisfy Nyquist sampling theorem, which was less than half wavelength at 9.3 GHz. The scanning areas are all 400 mm×400 mm, which had been chosen to capture the electric-field distribution and converted the results into the desired amplitude and phase distribution by the software in the control computer in real-time after measurement. The measured results are the same as simulated results which verify the method for multi-OAM-beam generation. The proposed method has potential in multi-platform wireless communication systems and the multi-channel imaging systems.

Fig. S4 Prototypes of DCTMS with different characteristics.